THE JOURNAL OF BIOLOGICAL CHEMISTRY VOL. 291, NO. 10, pp. 5309–5319, March 4, 2016

Base and Nucleotide Excision Repair of Oxidatively Generated Guanine Lesions in DNA*

Received for publication, September 17, 2015, and in revised form, January 4, 2016 Published, JBC Papers in Press, January 5, 2016, DOI 10.1074/jbc.M115.693218

Vladimir Shafirovich[‡1], Konstantin Kropachev[‡], Thomas Anderson[‡], Zhi Liu[‡], Marina Kolbanovskiy[‡], Brooke D. Martin[§], Kent Sugden[§], Yoonjung Shim[¶], Xuejing Chen[¶], Jung-Hyun Min[¶], and Nicholas E. Geacintov[‡2]

From the [‡]Department of Chemistry, New York University, New York, New York 10003, [§]Department of Chemistry, University of Montana, Missoula, Montana 59812, and [¶]Department of Chemistry, University of Illinois, Chicago, Illinois 60607

The well known biomarker of oxidative stress, 8-oxo-7,8-dihydroguanine, is more susceptible to further oxidation than the parent guanine base and can be oxidatively transformed to the genotoxic spiroiminodihydantoin (Sp) and 5-guanidinohydantoin (Gh) lesions. Incubation of 135-mer duplexes with single Sp or Gh lesions in human cell extracts yields a characteristic nucleotide excision repair (NER)-induced ladder of short dual incision oligonucleotide fragments in addition to base excision repair (BER) incision products. The ladders were not observed when NER was inhibited either by mouse monoclonal antibody (5F12) to human XPA or in XPC$^{-/-}$ fibroblast cell extracts. However, normal NER activity appeared when the XPC$^{-/-}$ cell extracts were complemented with XPC-RAD23B proteins. The Sp and Gh lesions are excellent substrates of both BER and NER. In contrast, 5-guanidino-4-nitroimidazole, a product of the oxidation of guanine in DNA by peroxynitrite, is an excellent substrate of BER only. In the case of mouse embryonic fibroblasts, BER of the Sp lesion is strongly reduced in NEIL1$^{-/-}$ relative to NEIL1$^{+/+}$ extracts. In summary, in human cell extracts, BER and NER activities co-exist and excise Gh and Sp DNA lesions, suggesting that the relative NER/BER product ratios may depend on competitive BER and NER protein binding to these lesions.

The overproduction of free radical intermediates and electrophiles by macrophages and neutrophils activated during the inflammatory response in chronically inflamed tissues induces persistent damage to cellular DNA (1). If not properly repaired, this DNA damage can increase levels of mutations and genomic instability and eventually can lead to the initiation of human cancers (2–4). The primary target of oxidatively generated DNA damage is guanine (5), the most easily oxidizable natural nucleic acid base (6). The best known oxidation product of guanine is 8-oxo-7,8-dihydroguanine (8-oxoG),[3] which is ubiquitous in cellular DNA and is used widely as a biomarker of oxidative stress (7). The 8-oxoG lesion is genotoxic, and failure to remove 8-oxoG before replication induces G:C → T:A transversion mutations (8). This lesion is even more easily oxidized than the parent base guanine (9), and its further oxidation by various oxidizing agents, including peroxynitrite, leads to the formation of stereoisomeric spiroiminodihydantoin (Sp) and 5-guanidinohydantoin (Gh) lesions (10–15). In the case of guanine oxidation by peroxynitrite, the 5-guanidino-4-nitroimidazole (NIm) lesion (16–18) is also produced and can serve as a biomarker of inflammation-related oxidation mechanisms (1). The NIm lesions together with the easily depurinated 8-nitroguanine, are typical products of guanine damage in calf thymus DNA induced by reactions with nitrosoperoxycarbonate (16, 19) derived from the combination of carbon dioxide and peroxynitrite (20). The structures of these oxidatively generated guanine lesions are shown in Fig. 1*A*.

The chiral carbons in the Gh and Sp nucleobases give rise to a pair of *R* and *S* diastereomers. Oligonucleotides that contain single, site-specifically inserted Gh or Sp lesions can be separated and purified by anion-exchange HPLC methods (21). In aqueous solutions, the Gh diastereomers are easily interconvertible, and it is, therefore, not feasible to study their characteristics individually (22). In contrast, the Sp-*S* and Sp-*R* diastereomers are chemically stable and can be purified and studied individually (10, 23). NMR structural studies in solution indicate that both stereoisomerically distinct Sp lesions (24) perturb adjacent base pairs and thus thermodynamically destabilize oligonucleotide duplexes (25). Molecular modeling studies indicate that the NIm lesions adopt flexible and multiple ring-opened structures with the nitro and guanidino groups, providing multiple hydrogen bonding possibilities (26).

The Gh and Sp lesions are highly mutagenic, resulting in G → C and G → T transversion mutations (27). The accumulation of Sp lesions was detected in Nei-deficient *Escherichia coli* after treatment of these cells with chromate (28) and were also detected in both the liver and colon tissues of *Rag*2$^{-/-}$ mice at levels ~100 times lower than those of 8-oxoG (29). Although the cellular levels of hydantoin lesions are low, these lesions can contribute to the malignant transformations of cells

* This work was supported by NIEHS, National Institutes of Health Grant RO1 ES 011589 (to V. S.) and RO1 ES 014872 (to K. S.). Components of this work were conducted in the Shared Instrumentation Facility at NYU that was constructed with support from a Research Facilities Improvement Grant (C06 RR-16572) from the National Center for Research Resources, National Institutes of Health. The authors declare that they have no conflicts of interest with the contents of this article.

[1] To whom correspondence may be addressed: Dept. of Chemistry, New York University, 31 Washington Place, New York, NY 10003-5180. Tel.: 212-998-8456; Fax: 212-995-4205; E-mail: vs5@nyu.edu.

[2] To whom correspondence may also be addressed: Dept. of Chemistry, NY University, 31 Washington Place, New York, NY 10003-5180. Tel.: 212-998-8407; Fax: 212-995-4205; E-mail: ng1@nyu.edu.

[3] The abbreviations used are: 8-oxoG, 8-oxo-7,8-dihydroguanine; Sp, spiroiminodihydantoin;Gh,5-guanidinohydantoin;NIm,5-guanidino-4-nitroimidazole; B[*a*]P-dG, 10*R* (+)-*cis-anti*-B[*a*]P-*N*^{2}-dG adduct; AP, apurinic/apyrimidinic; MEF, mouse embryonic fibroblasts; NER, nucleotide excision repair; BER, base excision repair.

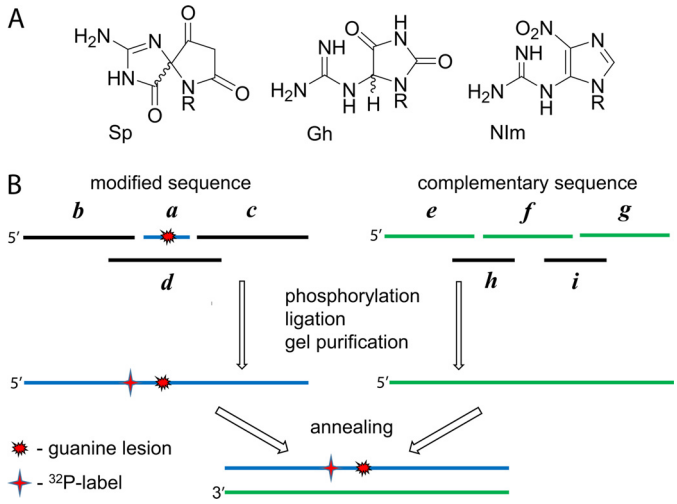

FIGURE 1. **BER and NER substrates.** *A*, structures of the oxidatively generated Sp, Gh, and NIm lesions. *B*, construction of the ^{32}P-internally labeled 135-bp duplexes containing site-specifically positioned guanine lesions. *a*, 11-mer 5′-CCATCXCTACC, where *X* = Sp-*S*, Gh, NIm, *cis*-B[*a*]P-N^2-dG. *b*, 62-mer 5′-GACCTGAACACGTACGGAATTCGATATCCTCGAGCCAGATCTGCGCCAGCTG-GCCACCC CCA. *c*, 62-mer 5′-ACCCGCCAAGCTTGGGCTGCAGCAGGTCGACTC-TAGAGGATCCCGGGCGAGCTCGAATTCGC. *d*, 31-mer 5′-CTTGGCGCTCGGTA-GCGATGGTCAGGGTGGC. *e*, 56-mer 5′-GCGAATTCGAGCTCGCCCGGGA-TCCTCTAGAGTCGACCTGCTGCAGCCCAAGCTTG. *f*, 27-mer 5′-GCGGGTGGTA-GCGATGGTGGGGGTGGC. *g*, 52-mer 5′-CAGCTGGCGCAGATCTGGCTCGAGG-ATATCGAATTCCGTACGTGTTCAGGTC. *h*, 20-mer 5′-TACCACCCGCCAAGCTT-GGG. *i*, 20-mer 5′-GCGCCAGCTGGCCACCCCCA.

because they are at least 1 order of magnitude more mutagenic than 8-oxoG (27). Mangerich *et al.* (29) found a correlation between the cellular levels of Sp lesions and the progression of disease in a mouse model of inflammation-induced colon cancer.

In vitro, the hydantoin lesions are efficiently repaired by base excision repair (BER) enzymes that include the *E. coli* Fpg (30), Nei (31), mammalian NEIL1 and NEIL2 (32), NEIL3 (33–36), human NEIL1 (37, 38), and NEIL3 (39) DNA glycosylases and by the prokaryotic nucleotide excision (NER) mechanism initiated by UvrABC proteins (40).

Here, we demonstrate that the incubation of site-specifically modified oligonucleotide duplexes containing single Sp or Gh lesions are excised by the human NER and BER systems when incubated in cell-free HeLa S3 cell extracts, whereas NIm is resistant to NER but is a substrate of BER.

Experimental Procedures

The oligonucleotide adducts containing the diastereomeric Sp lesions were generated by the site-selective oxidation of guanine nucleobase in 5′-CCATC**G**CTACC sequences with photochemically generated carbonate radical anions at pH 7.5–8.0 and isolated by anion-exchange HPLC methods (21, 25). The oligonucleotide 5′-CCATC(**Sp**)CTACC adduct containing the Sp-*S* diastereomer (Sp1) was the first-eluting fraction, whereas oligonucleotides with the Sp-*R* diastereomer (Sp2) eluted in the second fraction on a DNAPac PA-100 column (Dionex, Sunnyvale, CA) (24). The Gh-modified oligonucleotides were prepared by oxidation of the oligonucleotide 5′-CCATC(**8-oxoG**)-CTACC adducts with $(NH_4)_2IrCl_6$ complex at pH 6.0 (12, 21). The oligonucleotides with single NIm lesions were generated by oxidation of guanine in the same 5′-CCATC**G**CTACC sequence context using a photochemical method to generate carbonate radical anion/nitrogen dioxide radical species at pH 7.5–8.0 and isolated by reversed-phase HPLC (17, 41). As a positive control of NER activity we utilized duplexes containing the 10*R* (+)-*cis*-*anti*-B[*a*]P-N^2-dG adduct (abbreviated as B[*a*]P-dG) that are excellent substrates of the human NER system (42, 43). Oligonucleotides containing the stereochemically defined *cis*-B[*a*]P-N^2-dG adducts were used as markers of NER activity in cell extracts. These bulky adducts were generated by reacting the racemic diol epoxide (±)-*anti*-7,8-dihydroxy-9,10-epoxy-7,8,9,10-tetrahydrobenzo[*a*]pyrene diol epoxide with the 11-mer sequence 5′-CCTACGCTACC as described earlier (44). The 135-mer DNA strands containing the G-lesion at the 68th position from the 5′-end were generated by ligating the 5′-^{32}P-end-labeled 11-mer 5′-CCATC*X*CTACC (*X* = Sp-*S*, Gh, NIm, or B[*a*]P-dG) to 5′- and 3′-flanking 62-mers (43), purified by denaturing gel electrophoresis, and annealed with fully complementary 135-mer strands containing a C opposite X in the modified strand (Fig. 1*B*).

The HeLa S3 cells were purchased from American Type Culture Collection (Manassas, VA). SV40-transformed XP4PA-SV-EB fibroblasts deficient in XPC (GM15983) and the fully XPC-competent (GM16248) fibroblasts also derived from XP4PA-SV-EB (GM15983) by stable transfection with XPC-cDNA using the plasmid pXPC3 were purchased from the Coriell Institute for Medical Research (Camden, NJ). The cells were maintained according to the manufacturer protocols. Mouse monoclonal antibody (5F12) against human XPA (ab65963, Abcam, Cambridge, MA) was used to inhibit the NER activities. The full-length (amino acid residues 1–940) and truncated forms of XPC-RAD23B (the latter missing residues 1–155 only but active in binding to DNA (45)) were expressed in SF-9 insect cells as described (46). Another sample of full-length XPC-RAD23B was kindly provided by Dr. Orlando Schärer (Stony Brook University, Stony Brook, NY). Murine NEIL1 enzyme containing C-terminal His_6 tag was cloned, expressed, and purified as described previously (32, 47). Active site concentrations of the NEIL1 samples were determined using the Sp-*S* duplex as a substrate (37, 48).

Mouse embryonic fibroblasts (MEFs) from normal, BER-proficient, wild type mice (NEIL1$^{+/+}$) and homozygous knock-out mice (NEIL1$^{-/-}$) were provided by Dr. Stephen Lloyd (Oregon Health and Science University, Portland, OR). Cells were maintained in Dulbecco's modified Eagle's medium (Gibco) with 10% fetal calf serum gold (PAA Laboratories, MA) and 1% antibiotic/antimycotic solution (Gibco) at 37 °C and 5% CO_2. Knock-out cells were maintained and used at the lowest possible passage number (<7) due to the instability of the knock-out cell line (49). Cells were grown to 70–80% confluence, and (6–13) × 10^6 cells were harvested by trypsinization, washed twice with phosphate-buffered saline, and flash-frozen in liquid nitrogen.

The full details of the DNA repair experiments in extracts from HeLa S3 cells are described in detail elsewhere (50, 51). Briefly, the 50-μl reaction mixtures contained an ~1 nM concentration of the ^{32}P-internally labeled 135-bp duplexes with or without a lesion or adduct in a standard buffer solution (25 mM HEPES-KOH, pH 7.9, 0.1 M KCl, 12 mM $MgCl_2$, 1 mM EDTA,

17% glycerol, 2 mM DTT, and 2 mM ATP) containing 20–30 μg of protein from the cell extracts. The reactions were stopped after the desired incubation time by the addition of SDS to a concentration of 0.5% proteinase K (0.4 gm/ml), and this mixture was incubated for 1 h at 45 °C. The oligonucleotide excision products and intact 135-bp DNA duplexes were isolated by ethanol precipitation, subjected to denaturing 12% polyacrylamide gel electrophoresis, and analyzed by gel autoradiography using a Typhoon FLA 9000 laser scanner, and densitometric traces were generated from the autoradiographs using the ImageQuant software.

Results and Discussion

BER and NER Activities Are Observable in the Same Human Cell Extract DNA Repair Assays—The hallmark of successful NER activity in cell extracts is the appearance of ^{32}P-labeled oligonucleotides that are generally 24–32 nucleotides in length that contain the lesions (52, 53). In contrast, glycosylases cleave the *N*-glycosidic bond of the damaged base, thus resulting in the formation of an apurinic/apyrimidinic (AP) site in the damaged strand. The AP site is cleaved by lyase action, thus giving rise to a strand break at the site of the lesions (54) that results in the appearance of 67-mer incision products.

Typical results of the DNA repair assays in HeLa cell extracts obtained with 135-mer oligonucleotide duplexes containing single Sp-*S*, Gh, or NIm lesions are depicted in the autoradiograph of denaturing polyacrylamide gels shown in Fig. 2*A*. The electrophoretic migration distances of oligonucleotide size markers and their lengths (expressed in terms of numbers of nucleotides per strand) are shown in *lane 1* (Fig. 2*A*). The results shown in this gel were obtained from experiments that were conducted with aliquots from the same cell extract and at the same time; it is, therefore, possible to evaluate the relative incision activities of different substrates from such gels. After incubation of the 135-bp duplexes with the B[*a*]P-dG adducts for 15 and 30 min, the characteristic ladders of NER dual incision products of ~24–30 nucleotides in lengths are clearly visible in the case of the bulky B[*a*]P-N^2-dG adducts (Fig. 2*A*, *lanes 5* and *6*). These observations demonstrate that this cell extract was NER-active (42, 43). Using the same cell extract, a similar series but somewhat shorter oligonucleotide bands were observed in the case of the non-bulky Gh (*lanes 9–11*) and Sp-*S* lesions (*lanes 19–21*). These bands are also attributed to NER as shown in more detail below. However, analogous bands were not observed in the case of NIm (*lanes 13–16*), which thus appears to be NER-resistant. The repair efficiencies using duplexes containing the other Sp diastereomer, Sp-*R*, yielded qualitatively similar results (Fig. 3*A*).

The 135-bp duplexes with Sp, Gh, and NIm lesions are also incised at the sites of the lesions, thus generating ^{32}P-labeled 67-mer oligonucleotide fragments (Figs. 2*A* and 3*A*) that are attributed to BER activity (see below). However, there are no analogous 67-mer bands in the case of the bulky B[*a*]P-dG-modified duplexes that are not substrates of BER (Fig. 2*A*). The zero incubation time points in *lanes 2*, *7*, *12*, and *17* (Fig. 2*A*) represent control experiments (incubations in cell extracts were terminated within the first 20–25 s after manual mixing, and the samples were subjected to the same post-incubation treatment as all of the other samples). It is evident that the extent of observable incisions is negligible. A full set of controls with unmodified 135-mer duplexes incubated in cell extracts for different time intervals up to 60 min is shown in Fig. 4, *lanes 2–5*). Neither BER nor NER bands were observed in any of these control experiments.

Examples of densitometry traces derived from Fig. 2*A* at the 30-min incubation time points (*lanes 11*, *21*, and *16* for the Gh, Sp-*S*, and NIm samples, respectively) are depicted in Figs. 2, *B–D*. The relative yields of the 67-mer BER and the shorter NER products can be determined separately as a percentage of the initial 135-mer DNA strands incised. Because the repair activities are known to vary in different cell extract preparations, the BER and NER yields were normalized with respect to the Sp-*S* yield that was assigned an arbitrary value of 100 in each of the three independent experiments (the actual fractions of duplexes incised by the NER mechanisms were in the range of 7–25%). The averaged relative NER and BER yields derived from these three independent experiments in different cell extracts are summarized in Fig. 2*E*. In the case of the NER yields, the standard deviations indicate that there are no significant differences between the Sp, Gh, and B[*a*]P-dG lesions. In each of the individual cell extract experiments (Fig. 2*A*), the NER yields in the case of the B[a]P-dG adduct, Sp-*S*, and Gh lesions did not vary by $>\pm 20\%$. Similar variations were noted in the case of the BER yields observed with the Gh, Sp-*S*, and NIm lesions (Fig. 2, *B–D*). However, there were significantly higher variations in the [NER(B[*a*]P-dG,Sp-*S*,Gh)]/[BER(Sp-*S*,Gh-,NIm)] product yield ratios that ranged from 0.5 to 2.0 among the three individual cell extract experiments (Fig. 2*E*). Additional examples of the variabilities of the BER relative to the NER incisions are shown in Fig. 3, *B–D*, for the case of the stereoisomeric Sp-*R* lesion. These variations are also evident in the averaged BER yields that reflect the large standard deviations between the individual experiments (*blue bars* in Fig. 2*E*).

Electrophoretic Mobilities of NER Dual Incision Products—The group of dual incision products observed in the case of the Gh and Sp lesions (Fig. 2*A*) appear to migrate faster (*lanes 10* and *11* and *lanes 20* and *21*) than those containing the bulky B[*a*]P-dG adducts (*lanes 5* and *6*). The difference in mobilities of the single-stranded oligonucleotides with Gh and Sp-*S* lesions relative to those of the B[*a*]P-dG-modified excision products were further investigated. We synthesized 23-mer oligonucleotide strands containing either Sp or B[*a*]P-dG lesions. The 23-bp duplexes constructed from the ^{32}P-labeled B[*a*]P-dG and Sp-*S* sequences and the corresponding complementary strands were mixed with an excess of the unlabeled 135-bp duplexes, incubated with HeLa cell extracts for fixed periods of time (0, 30, and 60 min), and analyzed by denaturing polyacrylamide gel electrophoresis (Fig. 4, *lanes 7–15*). The 23-mer oligonucleotides with Sp-*S* lesions (*lanes 9*, *12*, and *15*) migrate approximately like 21-mer unmodified oligonucleotides (*lane 6*). This difference in mobilities (Fig. 4) is too small to account for the observed Sp and Gh NER fragments that are as short as 18–19 nucleotides (Fig. 2). However, Sugasawa *et al.* (55) showed earlier that the NER excision products of DNA with the UV light-induced cyclobutane thymine-thymine dimers and 6-4 pyrimidine-pyrimidone photoproducts exhibit similar

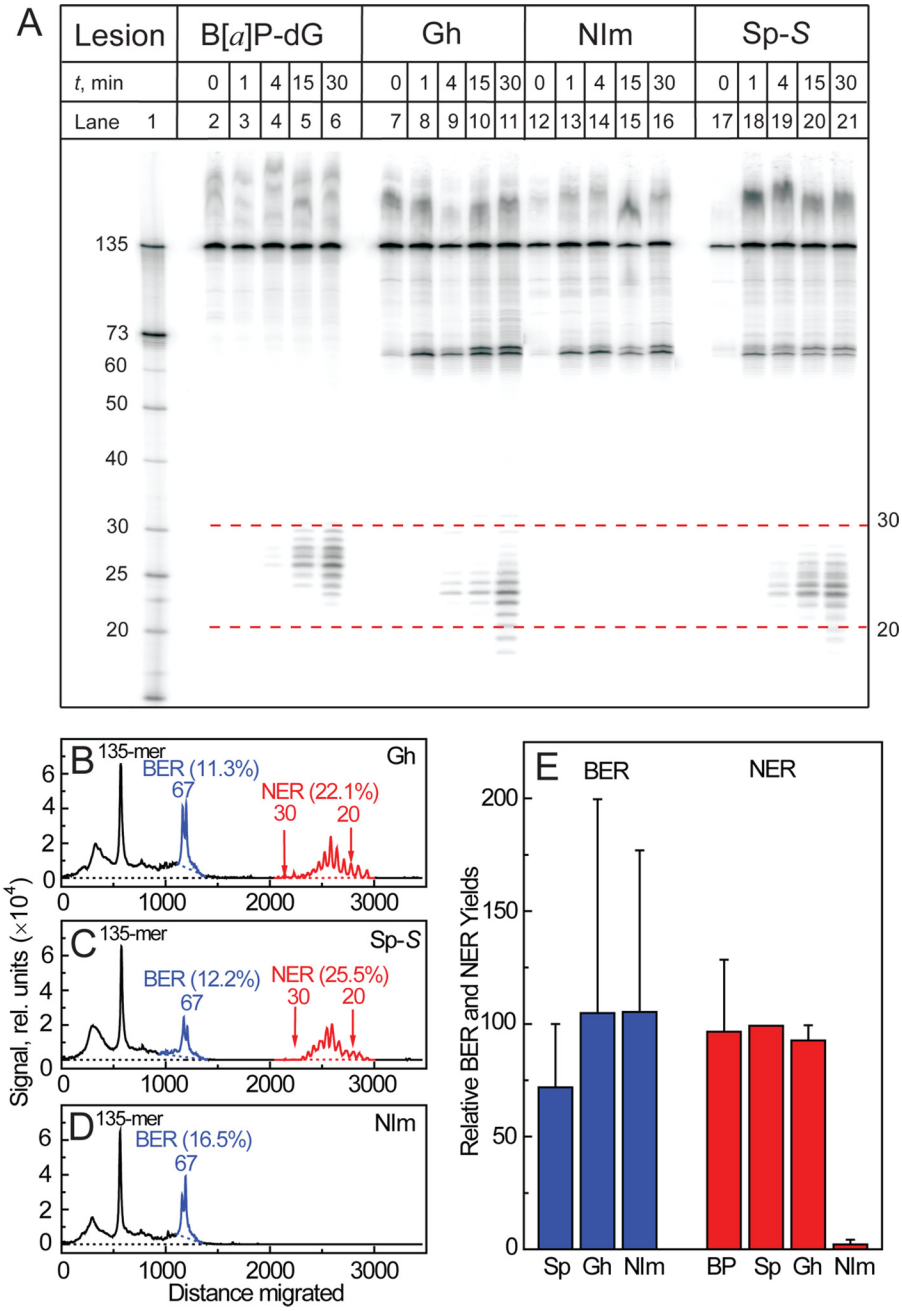

FIGURE 2. **BER incisions and NER dual incisions of 135-mer DNA duplexes with Gh, Sp-*S*, NIm, or B[*a*]P-dG lesions in cell-free extracts from HeLa cells.** *A*, representative denaturing gel showing the appearance of excision (BER) and dual incision (NER) products elicited by the Gh, Sp-*S*, and NIm-containing 135-bp duplexes (1 nM) as a function of incubation time in the same HeLa cell extract (0, 1, 4, 15, and 30 min). The 10*R* (+)-*cis*-*anti*-B[*a*]P-N^2-dG adducts were used as positive controls of NER activity. *Lane 1*, oligonucleotide size markers. The apparent size range of the NER dual incision products is shown by *dotted lines* (*red*). *B–D*, histograms derived from the gel autoradiograph (*A*, *lanes 11*, *16*, and *21*) depicting the relative distributions of BER and NER excision products in the 135-bp duplexes containing Gh (*B*), Sp-*S* (*C*), and NIm (*D*) lesions after incubation in the same HeLa cell extracts for 30 min. *E*, average NER (*red*) and BER (*blue*) yields based on three independent experiments, each in a different cell extract measured after a 30-min incubation period. In each of these individual experiments, the NER yields of Gh, NIm, and B[a]P-dG and the BER yields of Sp-*S*, Gh, and NIm lesions were normalized to the Sp-*S* NER value (arbitrarily assigned the value of 100) in the same experiment. The *blue* and *red bars* represent the averages of the three independent experiments with their standard deviations. Other details are described in "Experimental Procedures."

patterns of dual incision products that are <25 nucleotides in lengths. Huang *et al.* (56, 57) reported earlier that in cell extracts NER excision products are progressively degraded to shorter oligonucleotides as the incubation time is increased, thus shifting the group of NER dual incision products farther down the gel autoradiographs. Therefore, the faster-migrating ladder of bands in the case of the dual incision products (Fig. 2*A*) observed in the case of the Gh and Sp-*S* lesions (*lanes 10* and *11* and *20* and *21*) relative to the slower mobility bands with B[*a*]P-dG adducts (*lanes 5* and *6*) can be attributed to (i) an intrinsic faster electrophoretic mobility of the Gh- and Sp-modified short oligonucleotides in comparison with the same length B[*a*]P-dG fragments, and (ii) the partial degradation of the excised oligonucleotides by nonspecific nucleases

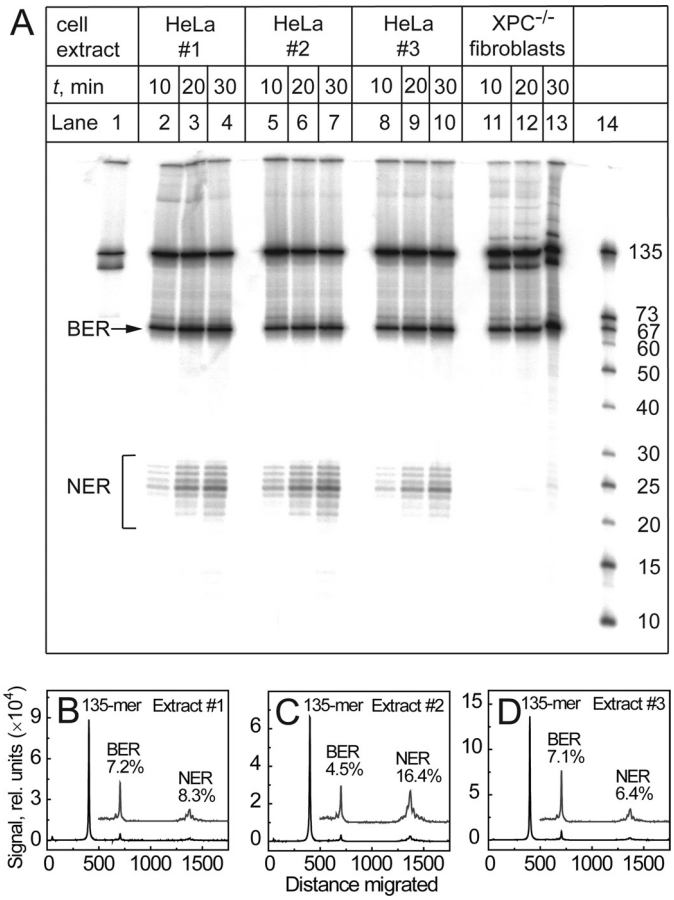

FIGURE 3. **BER and NER of Sp-*R* lesions in HeLa cell extracts and XPC-proficient or XPC-deficient fibroblasts.** *A*, three additional examples of single (BER) and dual (NER) incisions elicited by the stereoisomeric Sp-*R* lesions containing 135-bp duplexes as a function of incubation time (10, 20, and 30 min) in HeLa cell extracts (three different preparations) and extracts from XPC-deficient ($XPC^{-/-}$) cells. *Lane 14*, oligonucleotide size markers. *B–D*, histograms derived from the gel autoradiograph (*A*) depicting the relative distributions of BER and NER excision products in the 135-bp Sp-*R* duplexes after incubation in three different preparations of HeLa cell extracts for 30 min.

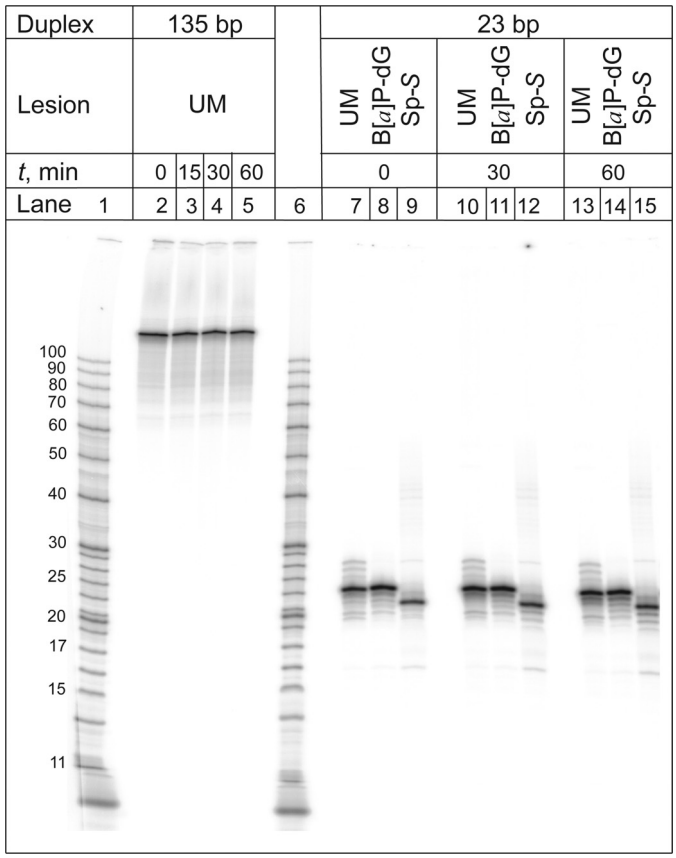

FIGURE 4. **Denaturing gel showing different electrophoretic mobilities of single-stranded 23-mer oligonucleotides without (unmodified) and with single B[*a*]P-dG adducts or Sp-*S* lesions.** In total, eight such experiments were performed that showed qualitatively similar behavior. The 23-bp duplexes were constructed from 5′-TGGCCACCCTGA*CCATC*X*CTACC oligonucleotides with the ^{32}P internal label at position indicated by an *asterisk* (*) and *X* = G, B[*a*]P-dG, or Sp-*S*. These 23-mer sequences (1 nM) were annealed with their fully complementary 23-mer strands containing a C opposite *X* in the modified strands, incubated in HeLa cell extracts with an excess of the unlabeled 135-bp duplexes (10 nM) for fixed periods of time (0, 30, and 60 min), and subsequently analyzed by denaturing gel electrophoresis. *Lanes 1* and *6*, oligonucleotide size markers. *UM*, unmodified 135-bp duplex control.

(56, 57) that gradually diminish the size of the NER dual incision products. The oligonucleotide dual incision products in the case of the bulky B[*a*]P-dG products appear to be more resistant to nuclease digestion. The resistance of B[*a*]P-dG adducts to digestion catalyzed by exonucleases was described earlier (58).

The Appearance of 67-Mer Incision Products in Mouse Embryonic Fibroblast Is Consistent with BER Activities—To further support the conclusion that the 67-mers are indeed BER excision fragments, the 135-bp Sp-*S* and Sp-*R* duplexes were incubated with extracts from MEF $NEIL1^{+/+}$ and $NEIL1^{-/-}$ cells (Fig. 5). These wild type and NEIL1 knock-out cells were selected because it is well established that the Sp lesions are substrates of NEIL1 *in vitro* (32). In Fig. 5 it is shown that the excision of Sp lesions is significantly reduced in $NEIL1^{-/-}$ cells (*lanes 3*, *6*, and *9*) relative to wild type cells (*lanes 4*, *7*, and *10*) in three different sequence contexts. Densitometric analysis shows that the reduction in activity is ~18-fold in these MEF $NEIL1^{-/-}$ cells. The Sp and Gh are good substrates of the Nei family glycosylases NEIL2 and NEIL3 *in vitro* (32, 39). It is, therefore, likely that the residual BER activity observed in extracts from $NEIL1^{-/-}$ cells (*lanes 3*, *6*, and *9*, Fig. 5) might be associated with the presence of DNA glycosylases other than NEIIL1. We note that these particular MEF cell extracts did not show any NER activity, although very weak activities were observed in some samples. By contrast, extracts from human fibroblasts do exhibit NER activities (see below), and thus studies of NER in MEF extracts were not further pursued.

Time Dependence of NER and BER Excision Activities—Examples of the BER and NER kinetics at different 135-bp Sp-*S* substrate concentrations are depicted in Fig. 6, *A* and *C*. In these figures the yields of excision products calculated by integration of the histograms derived from the denaturing gel autoradiographs (Fig. 2, *B–D*) are plotted as a function of incubation time in HeLa cell extracts. The NER kinetics are linear up to at least 45 min (Fig. 6*C*) but level off at higher incubation times (data not shown). In contrast, the BER kinetics shown in Fig. 6*A* are nonlinear in HeLa cell extracts. The yield of 67-mer excision products rises rapidly within the first 1–2 min followed by a much slower linear phase. These biphasic kinetics resemble classical base excision reaction kinetics that exhibit a rapid

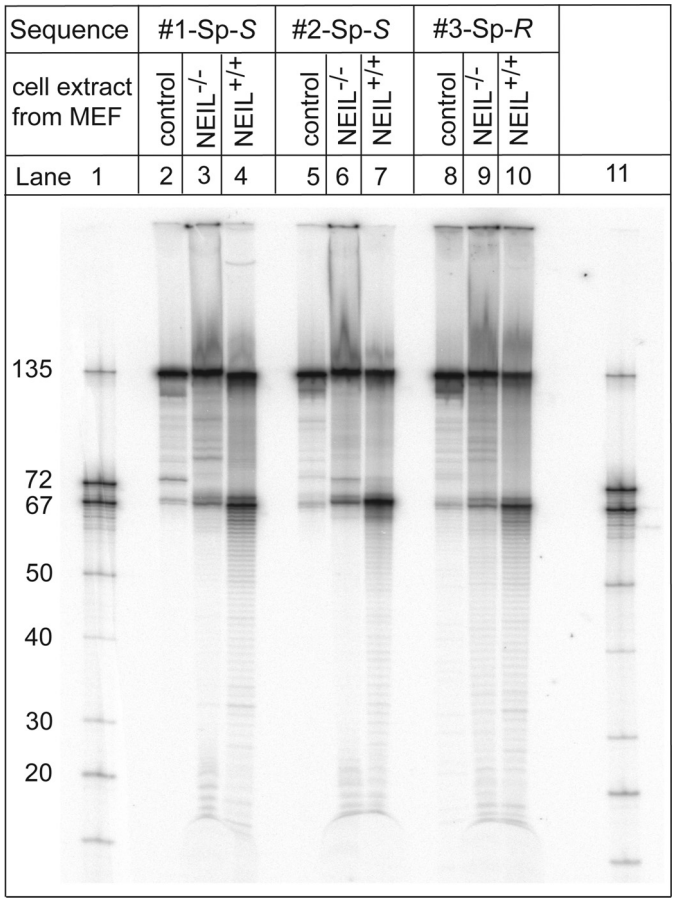

FIGURE 5. **BER activities of 135-bp duplexes with centrally positioned Sp lesions in cell-free extracts from wild (NEIL1$^{+/+}$) and KO (NEIL1$^{-/-}$) MEFs.** The 135-mer modified strands contained the centrally positioned sequences: 5-CCATC(Sp-*S*)CTACC (*#1*), 5′-CCACCAAC(Sp-*S*)CTACCACC (*#2*), or 5′-CCACCAAC(Sp-*R*)TCACCACC (*#3*); the remaining base sequences in the 135-mer duplexes with #2 and #3 are shown in Fig. 1*B*. *Lanes 1* and *11*, oligonucleotide size markers. The BER activities (yield of 67-mer fragments) are strongly reduced in NEIL1$^{-/-}$ sequences in all three sequence contexts.

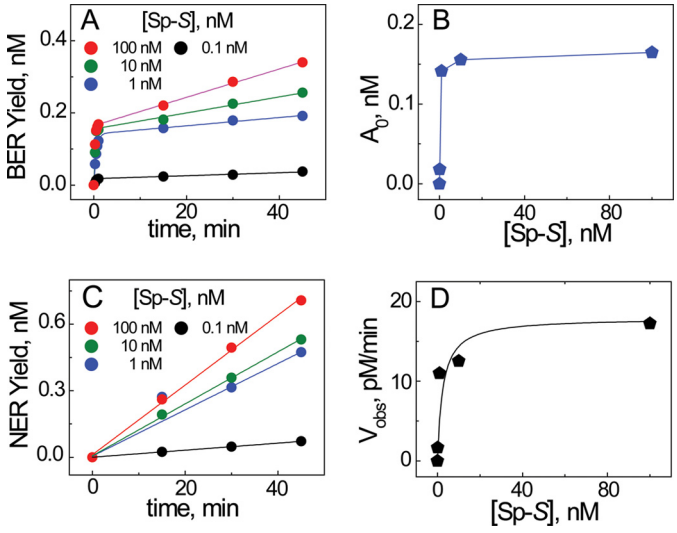

FIGURE 6. **Example of the kinetics of appearance of BER and NER incision product formation (*A* and *C*) and the effects of DNA substrate concentration (*B* and *D*).** The DNA substrate was a 135-bp duplex containing a single Sp-*S* lesions in HeLa cell extracts. Similar qualitative behavior was observed with four other cell extracts analyzed in detail, although the BER product yields were variable as discussed in connection with the *error bars* shown in Fig. 2*E* and the results in Fig. 3, *B–D*. *A*, time course of single incision 67-mer BER product formation. The *solid lines* are the least-squares fits of the BER Equation 1 to the experimental data points. *B*, dependence of the burst amplitude on the DNA substrate concentration; the *solid line* is meant to guide the eye only. *C*, time course of dual incision NER product formation. The *solid lines* are the least-squares linear fits to the data points. *D*, dependence of the dual excision yield at the 30-min incubation time point on the DNA substrate concentration. The *solid line* is a fit of the Michaelis-Menten equation, $V_{obs} = V_{max}[DNA_S]/(K_m + [DNA_S])$ with V_{max} = pM·min^{-1}, and K_m = 2.5 nM to the observed NER rates.

burst phase due to single turnover reactions followed by a linear steady-state phase that is determined by the rate of release of DNA BER incision products (37, 48, 59, 60).

It has been shown that BER activities in cell-free extracts from HeLa cells are associated with endonuclease VIII-like proteins (NEIL1, NEIL2, and NEIL3) (61–63) that cleave the *N*-glycosyl bonds of Sp/Gh lesions, thus generating abasic sites (32, 37, 39, 64–67). NEIL1 and NEIL2 are bifunctional DNA glycosylases that further cleave the abasic sites by the intrinsic lyase activity that results in the formation of 5′-side fragments with 3′-phosphate groups at the ends (via β,δ elimination) (54, 63). Therefore, the faster-migrating 67-mer oligonucleotide BER incision products (*lanes 8–11*, *13–16*, and *18–21*, Fig. 2*A*) can be assigned to the 5′-side cleavage fragments with 3′-phosphate ends (32, 37, 38). In HeLa cell extracts, the 3′-phosphate groups are removed by the phosphatase activity of polynucleotide kinases to form the slower migrating fragments with OH groups at the 3′-ends (68–70). Indeed, these slower migrating 67-mer fragments with 3′-OH ends (*lanes 9–11*, *14–16*, and *19–21*, Fig. 2*A*) were observed at longer incubation times (4–30 min), which was attributed to the pronounced phosphatase activity of these particular HeLa cell extracts (68). These 5′-side cleavage fragments with 3′-OH groups are not detected in BER experiments with Sp and Gh lesions conducted with purified NEIL1 and NEIL2 *in vitro* (32, 37, 38). However, NEIL3 does not seem to play a role in the BER activity shown in Fig. 2*A*. NEIL3 is a monofunctional glycosylase without intrinsic lyase activity and an AP endonuclease (APE1) is typically recruited to cleave the abasic site (63). The latter mechanism generates a 5′-side fragment formed that contains an α,β-unsaturated aldehyde group (β-elimination) at the 3′-ends. Such a 5′-fragment is not evident in our cell extract experiments (Fig. 2*A*) because its mobility would be even slower than that of a fragment with a 3′-OH group (70).

To gain further insights into the BER and NER processes, we analyzed the reaction kinetics at different concentrations of the Sp-*S* duplexes (Fig. 6). The biphasic kinetics (Fig. 6*A*) can be represented by the standard scheme used to describe kinetics of the base excision repair of Sp and Gh lesions *in vitro* by hNEIL1 (37), 8-oxoG by MutY (48), and hOGG1 (59), and thymine glycol by hNTH1 (60):

$$DNA_S + E_{BER} \overset{K_{BER}}{\longleftrightarrow} DNA_S \cdot E_{BER} \overset{K_{BER}}{\longrightarrow} DNA_P \cdot E_{BER} \overset{k_P}{\rightarrow} DNA_P + E_{BER}$$

Reaction 1

Under multiple turnover conditions the concentration of the DNA substrate exceeds that of the enzyme, ($[DNA_S] > [E_{BER}]_0$), and the yield of BER products is characterized by a fast

burst of product formation (amplitude A_0) with the observed rate constant (k_{obs}) followed by a slower, steady-state linear phase with the slope (k_{ss}) (Fig. 6*A*). The kinetics of the appearance of DNA cleavage products ($[DNA_P]_t$) as a function of time (t) is described by the classic burst equation,

$$[DNA_P] = A_0\{1 - \exp(-k_{obs}t)\} + k_{ss}t \qquad \text{(Eq. 1)}$$

An increase in the concentration of the DNA substrate leads to increases of the values of A_0 and k_{ss}, and in the high concentration limit $A_0 = [E_{BER}]_0$, $k_{obs} = k_{BER}$, and $k_{ss} = k_P[E_{BER}]_0$, where k_{BER} is the rate constant of the chemical reaction in the enzyme-(DNA substrate) complex ($DNA_S{\cdot}E_{BER}$), whereas k_P is the rate constant of product release from the enzyme-(DNA product) complex, ($DNA_P{\cdot}E_{BER}$) (48). The overall BER product yield as a function of DNA concentration in HeLa cell extract is consistent with these predictions (Fig. 6, *A* and *B*). The results shown in Fig. 6*B* indicate that the burst amplitude does not significantly increase at DNA substrate concentrations above $[DNA_S] > 10$ nM, which provides an approximate value of $[E_{BER}]_0 = 0.15–0.19$ nM BER enzyme concentration in this example. In terms of this scheme, the active concentrations of BER enzymes in HeLa cell extract are almost the same for all three BER substrates studied (Sp-*S*, Gh, and NIm) (data not shown). The values of the burst phase rate constant, k_{BER}, are too high to be kinetically resolvable under our experimental conditions that are based on manual mixing procedures; using rapid quench flow techniques, values of $k_{BER} \sim 100–180$ min^{-1} were determined for the excision of Gh and Sp lesions by hNEIL1 *in vitro* (37).

The NER dual incision kinetics are linear up to at least 45 min (Fig. 6*C*) as shown earlier in the case of the cyclobutane thymine-thymine dimers and 6–4 pyrimidine-pyrimidone photoproducts as well as other DNA lesions in cell extracts (50) and in cells (71). Increasing the concentration of the DNA substrate enhances the observed rate of NER product formation,

$$V_{obs} = \Delta[DNA_p]/\Delta t \qquad \text{(Eq. 2)}$$

calculated from the linear portions of the product concentrations (Fig. 6*C*). Under these conditions, the value of V_{obs} became independent of the DNA substrate concentration and attained the maximum rate $V_{max} = k_{NER}[E_{NER}]_0$, which is ~18 pM·min^{-1} at $[DNA_S] > 10$ nM) in the particular HeLa cell extract described in this example (Fig. 6*D*).

XPC-RAD23B Complementation Experiments and Impact of a Monoclonal XPA Antibody on NER Activity—The eukaryotic and heterodimeric protein XPC-RAD23B binds stably to a variety of DNA lesions and is a critical factor in NER (72, 73). The XPC-RAD23B binding step initiates the cascade of NER steps that ultimately result in the appearance of the dual incision fragments (74, 75). In some cases DDB is required for the recruitment of XPC. This effect is well established in whole cells (for review, see Ref. 74). However, *in vitro*, a role of DDB has been proposed for specific lesions like cyclobutane pyrimidine dimers under some conditions but not in others (74). The importance of XPC-RAD23B is supported by the observation that the 20–27-mer products generated by NER activity are absent when the 135-bp duplexes containing Sp-*S* (*lane 5*, Fig. 7) or Sp-*R* (Fig. 3) are incubated in whole cell extracts from XPC$^{-/-}$ fibroblasts that are not expressing XPC. In contrast, 67-mer fragments produced by BER activity are still observed, because XPC-deficiency affects only the NER activity. The extracts from HeLa cells and XPC$^{+/+}$ fibroblasts used as a positive control (*lanes 3* and *4*, Fig. 7) demonstrate a normal NER activity (as in Figs. 2 and 3). The NER activity of cell extracts from XPC$^{-/-}$ fibroblasts can be restored by the addition of XPC-RAD23B. Indeed, dual incision products are clearly observed after the addition of the XPC-RAD23B heterodimer assembled from full-length XPC (*lanes 7* and *8*, Fig. 7) but not from the truncated form of XPC that is missing amino acids 1–155 in the N-terminal region (*lane 6*, Fig. 7).

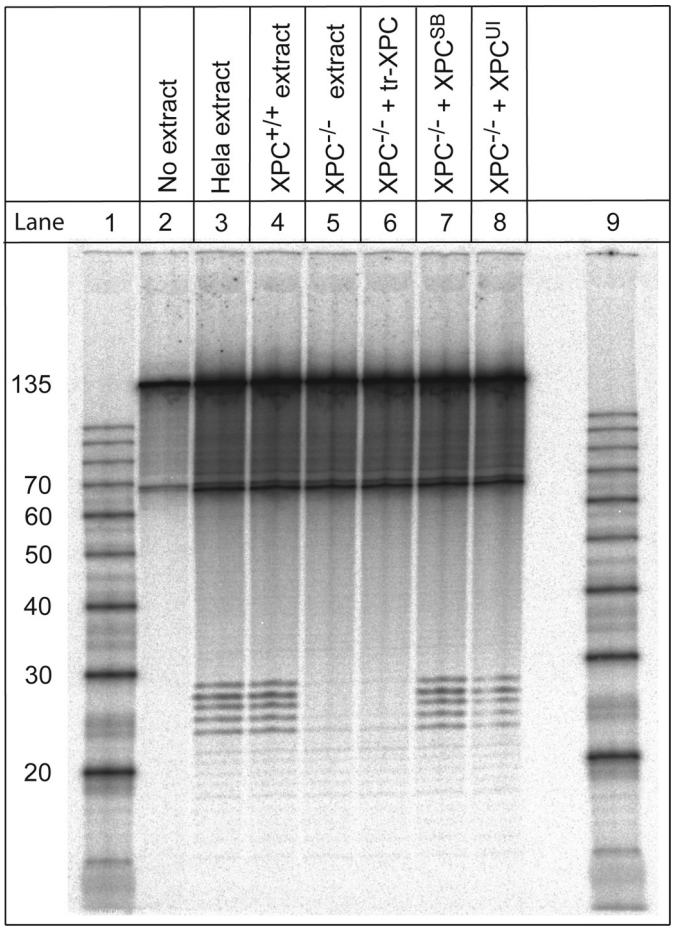

FIGURE 7. **XPC-RAD23B complementation experiments in XPC-deficient fibroblasts.** Representative denaturing gel electrophoresis of NER products after incubation of Sp-*S*-containing 135-bp duplexes (1 nM) in normal HeLa cell extracts (*lane 3*), extracts from XPC$^{+/+}$ fibroblasts (*lane 4*), extracts from XPC$^{-/-}$ cells (*lane 5*), extracts from XPC$^{-/-}$ cells complemented with 4 nM concentrations of truncated XPC-RAD23B (tr-XPC, *lane 6*), full XPC-RAD23B from Stony Brook University (XPC^{SB}, *lane 7*), or from the University of Illinois (XPC^{UI}, *lane 8*). *Lanes 1* and *9*, oligonucleotide size markers. The incubation times were 30 min in all experiments. In total, four such experiments were performed that showed qualitatively similar behavior.

Additional evidence that the appearance of the 20–27-mer oligonucleotide ladder is due to NER activity, which causes the observed dual incision activities of the Sp- and Gh-containing 135-mer duplexes, are the observations that the latter disappears in the presence of low concentrations of monoclonal antibody against XPA. This protein is a key component of the NER

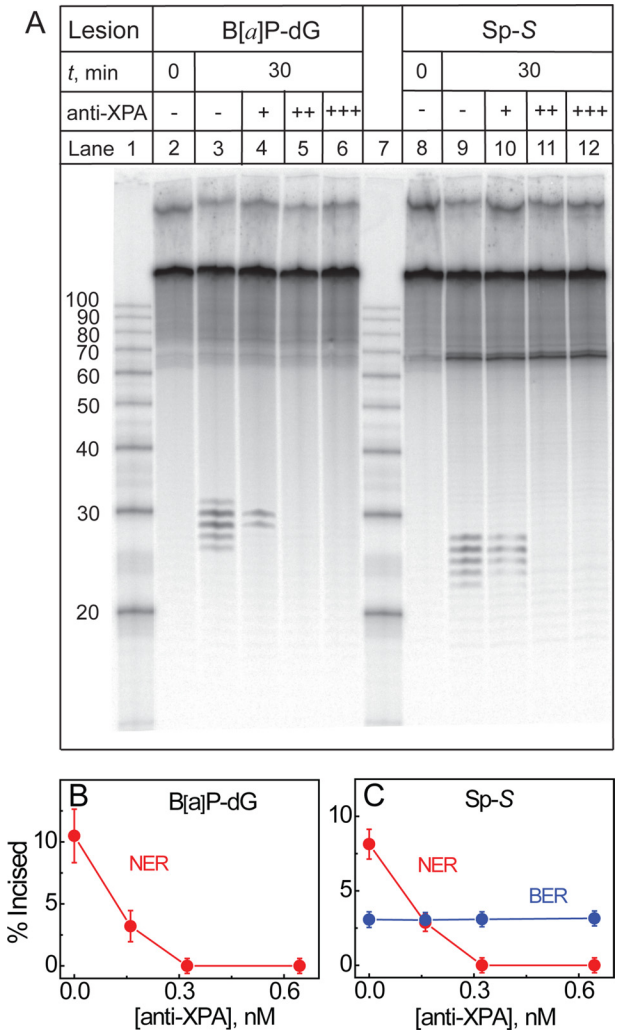

FIGURE 8. **Inhibition of NER activities of HeLa cell extracts by the addition of mouse monoclonal anti-XPA antibodies.** *A*, denaturing gel showing the inhibition of NER dual incision activity associated with 135-bp Sp-*S*-containing duplexes (1 nM) as a function of a mouse monoclonal anti-XPA (5F12) concentration after incubation in HeLa cell extracts for fixed periods of time (0 and 30 min). The 10*R* (+)-*cis*-*anti*-B[*a*]P-N^2-dG adduct embedded in 135-mers was used as a positive control of NER activity. *Lanes 1* and *7*, oligonucleotide size markers. *B* and *C*, average yields of BER (*blue*) and NER (*red*) BER incision and NER excision products measured at the 30-min incubation time point as a function of anti-XPA concentration (averages of three independent experiments).

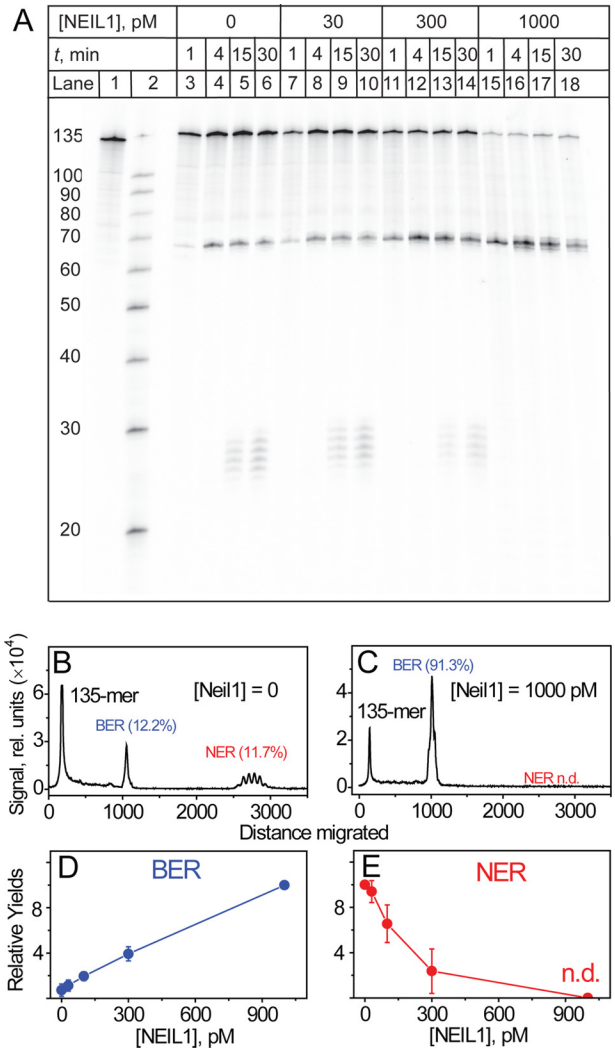

FIGURE 9. **Competition between BER and NER pathways in HeLa cell extracts.** *A*, autoradiograph of a denaturing gel showing the BER and NER product yields as a function of the concentration of the BER glycosylase NEIL1. The substrates were 135-bp duplexes (1 nM) containing single Sp-*S* lesions. *Lane 1*, DNA substrate not treated in cell extracts (control). *Lane 2*, oligonucleotide size markers. *B* and *C*, histograms derived from the gel autoradiograph (*A*, *lanes 6* and *18* at the 30-min incubation time point). *D*, average NER (*red*) and BER (*blue*) yields based on three independent experiments, each in different cell extracts measured after a 30-min incubation period. In each of these individual experiments the NER and BER yields of Sp-*S* were normalized either to the NER value at [NEIL1] = 0 or the BER value at [NEIL1] = 1000 pM (arbitrarily assigned a value of 10 in each case).

machinery (76), and inhibition of XPA activity by anti-XPA antibodies has been widely used for validating the existence of NER mechanisms (77–80). For example, the mouse monoclonal anti-XPA (5F12) antibody strongly inhibits NER of oxidatively generated 5′,8-cyclopurine lesions (78) and the 1,3-intrastrand d(GpTpG)-cisplatin cross-linked lesions (79). Indeed, the addition of anti-XPA (5F12) to the 135-bp Sp-*S* duplexes selectively inhibits the appearance of the dual incision products, whereas the 67-mer incision fragments produced by the BER activity remain at the same level (*lanes 10–12*, Fig. 8*A*). The B[*a*]P-dG adducts embedded in 135-mer duplexes are well established NER substrates (42, 43) and provide a positive control for validating the existence of NER mechanism in these experiments (*lanes 4–6*, Fig. 8*A*). The yields of dual incision products elicited either by the B[*a*]P-dG adducts (Fig. 8*B*) or by Sp-*S* lesions (Fig. 8*C*) decrease as the concentration of the XPA antibody is increased. The complete inhibition of the dual incision products at anti-XPA antibody concentrations of ~ 0.2–0.3 nM suggests that the XPA concentration in these HeLa cell extracts is in that range as well (Fig. 8, *B* and *C*).

It is remarkable that human NER and BER proteins can function in parallel in repairing Sp and Gh DNA lesions in human HeLa cell extract experiments. These observations suggest that these two pathways complement one another to maximize the efficiency of removal of these DNA lesions and may operate in whole cells as well.

Competition between BER and NER Pathways—Our working hypothesis is that the observation of parallel BER and NER activities in cell extracts is due to competitive BER and NER protein binding to the Gh and Sp substrates. According to this

hypothesis, the addition of increasing amounts of an exogenous BER glycosylase should enhance the yield of BER incisions, whereas the NER activity should decrease. This hypothesis is consistent with the competition experiments depicted in Fig. 9. Increasing the concentrations of the bifunctional BER glycosylase NEILI to cell extracts containing 135-bp duplexes with single Sp-*S* lesions decreased the NER product yields; the levels of the NER dual incision products became negligible at the highest concentrations of the BER glycosylase employed in these experiments (Fig. 9*E*). By contrast, the relative yield of the 67-nucleotide BER cleavage products increased markedly with increasing concentrations of NEIL1 (Fig. 9*D*). These results are attributed to a competition between NEIL1 and the initial NER DNA lesion recognition factor XPC-RAD23B for binding to the same DNA lesion that increasingly favors NEIL1 as its concentration is increased.

Mechanistic Considerations—An interesting question is why the NIm lesion is resistant to NER, whereas the structurally similar Gh lesion is an excellent NER substrate. The two lesions are distinguished from one another only by the replacement of the keto group in Gh by an -NO_2 group in NIm (Fig. 1). Molecular modeling studies indicate that the NIm lesions adopt flexible and multiple ring-opened structures with the nitro and guanidino groups providing multiple hydrogen bonding possibilities (26). By contrast, Gh can exist in the forms of two slowly interconverting *R* and *S* stereoisomers (81, 82). On the other hand, the stereoisomeric Sp structures exist as stable and identifiable *R* and *S* stereoisomers (24, 83). All three lesions, NIm, Gh, and Sp, cause significant thermodynamic destabilization of DNA duplexes (21, 25, 26, 82–87), which is a common feature of DNA substrates that are recognized by the NER machinery. Thus, the Sp and Gh lesions are recognized by the prokaryotic UvrABC nuclease (40) as well as by the eukaryotic NER machinery in human cell extracts as demonstrated here. However, the NER resistance of NIm appears to be correlated not with a destabilization but with its conformational flexibility in double-stranded DNA (26). It is noteworthy that the behavior of NIm lesions relative to Sp and Gh lesions is also quite different in translesion bypass experiments catalyzed by the human polymerase β (pol β); the NIm lesions are efficiently bypassed by pol β (16), whereas pol β is completely stalled by Sp and Gh lesions (88).

Author Contributions—K. K. and T. A. carried out the DNA repair experiments, Z. L. synthesized the site-specifically modified DNA lesions, M. K. generated the 135-mer duplexes, K. S. and B. M. provided the MEF NEILl wild type and knockout cells, Y. S., X. C., and J.-H. M. supplied the XPC-RAD23B proteins, and V. S. and N. E. G. supervised the experimental work and wrote the manuscript. All authors approved the final version of the manuscript.

Acknowledgments—Acquisition of the MALDI-TOF mass spectrometer was supported by the National Science Foundation (CHE-0958457).

References

1. Lonkar, P., and Dedon, P. C. (2011) Reactive species and DNA damage in chronic inflammation: reconciling chemical mechanisms and biological fates. *Int. J. Cancer* **128,** 1999–2009
2. Coussens, L. M., and Werb, Z. (2002) Inflammation and cancer. *Nature* **420,** 860–867
3. Grivennikov, S. I., Greten, F. R., and Karin, M. (2010) Immunity, inflammation, and cancer. *Cell* **140,** 883–899
4. Kidane, D., Chae, W. J., Czochor, J., Eckert, K. A., Glazer, P. M., Bothwell, A. L., and Sweasy, J. B. (2014) Interplay between DNA repair and inflammation, and the link to cancer. *Crit. Rev. Biochem. Mol. Biol.* **49,** 116–139
5. Cadet, J., Douki, T., and Ravanat, J. L. (2008) Oxidatively generated damage to the guanine moiety of DNA: mechanistic aspects and formation in cells. *Acc. Chem. Res.* **41,** 1075–1083
6. Steenken, S., and Jovanovic, S. V. (1997) How easily oxidizable is DNA? One-electron reduction potentials of adenosine and guanosine radicals in aqueous solution. *J. Am. Chem. Soc.* **119,** 617–618
7. Cadet, J., Douki, T., and Ravanat, J. L. (2010) Oxidatively generated base damage to cellular DNA. *Free Radic. Biol. Med.* **49,** 9–21
8. Bjelland, S., and Seeberg, E. (2003) Mutagenicity, toxicity, and repair of DNA base damage induced by oxidation. *Mutat. Res.* **531,** 37–80
9. Steenken, S., Jovanovic, S. V., Bietti, M., and Bernhard, K. (2000) The trap depth (in DNA) of 8-oxo-7,8-dihydro-2′-deoxyguanosine as derived from electron-transfer equilibria in aqueous solution. *J. Am. Chem. Soc.* **122,** 2373–2374
10. Luo, W., Muller, J. G., Rachlin, E. M., and Burrows, C. J. (2000) Characterization of spiroiminodihydantoin as a product of one-electron oxidation of 8-oxo-7,8-dihydroguanosine. *Org. Lett.* **2,** 613–616
11. Niles, J. C., Wishnok, J. S., and Tannenbaum, S. R. (2001) Spiroiminodihydantoin is the major product of the 8-oxo-7,8-dihydroguanosine reaction with peroxynitrite in the presence of thiols and guanosine photooxidation by methylene blue. *Org. Lett.* **3,** 963–966
12. Fleming, A. M., Muller, J. G., Dlouhy, A. C., and Burrows, C. J. (2012) Structural context effects in the oxidation of 8-oxo-7,8-dihydro-2′-deoxyguanosine to hydantoin products: electrostatics, base stacking, and base pairing. *J. Am. Chem. Soc.* **134,** 15091–15102
13. Burrows, C. J., Muller, J. G., Kornyushyna, O., Luo, W., Duarte, V., Leipold, M. D., and David, S. S. (2002) Structure and potential mutagenicity of new hydantoin products from guanosine and 8-oxo-7,8-dihydroguanine oxidation by transition metals. *Environ. Health Perspect.* **110,** 713–717
14. Sugden, K. D., Campo, C. K., and Martin, B. D. (2001) Direct oxidation of guanine and 7,8-dihydro-8-oxoguanine in DNA by a high-valent chromium complex: a possible mechanism for chromate genotoxicity. *Chem. Res. Toxicol.* **14,** 1315–1322
15. Cui, L., Ye, W., Prestwich, E. G., Wishnok, J. S., Taghizadeh, K., Dedon, P. C., and Tannenbaum, S. R. (2013) Comparative analysis of four oxidized guanine lesions from reactions of DNA with peroxynitrite, singlet oxygen, and γ-radiation. *Chem. Res. Toxicol.* **26,** 195–202
16. Gu, F., Stillwell, W. G., Wishnok, J. S., Shallop, A. J., Jones, R. A., and Tannenbaum, S. R. (2002) Peroxynitrite-induced reactions of synthetic oligo 2′-deoxynucleotides and DNA containing guanine: formation and stability of a 5-guanidino-4-nitroimidazole lesion. *Biochemistry* **41,** 7508–7518
17. Joffe, A., Mock, S., Yun, B. H., Kolbanovskiy, A., Geacintov, N. E., and Shafirovich, V. (2003) Oxidative generation of guanine radicals by carbonate radicals and their reactions with nitrogen dioxide to form site specific 5-guanidino-4-nitroimidazole lesions in oligodeoxynucleotides. *Chem. Res. Toxicol.* **16,** 966–973
18. Niles, J. C., Wishnok, J. S., and Tannenbaum, S. R. (2001) A novel nitroimidazole compound formed during the reaction of peroxynitrite with 2′,3′,5′-tri-*O*-acetyl-guanosine. *J. Am. Chem. Soc.* **123,** 12147–12151
19. Yun, B. H., Geacintov, N. E., and Shafirovich, V. (2011) Generation of guanine-thymidine cross-links in DNA by peroxynitrite/carbon dioxide. *Chem. Res. Toxicol.* **24,** 1144–1152
20. Goldstein, S., Lind, J., and Merényi, G. (2005) Chemistry of peroxynitrites as compared to peroxynitrates. *Chem. Rev.* **105,** 2457–2470
21. Kornyushyna, O., Berges, A. M., Muller, J. G., and Burrows, C. J. (2002) *In vitro* nucleotide misinsertion opposite the oxidized guanosine lesions spiroiminodihydantoin and guanidinohydantoin and DNA synthesis past the lesions using *Escherichia coli* DNA polymerase I (Klenow fragment). *Biochemistry* **41,** 15304–15314

22. Ye, Y., Muller, J. G., Luo, W., Mayne, C. L., Shallop, A. J., Jones, R. A., and Burrows, C. J. (2003) Formation of ^{13}C-, ^{15}N-, and ^{18}O-labeled guanidinohydantoin from guanosine oxidation with singlet oxygen. Implications for structure and mechanism. *J. Am. Chem. Soc.* **125,** 13926–13927
23. Ravanat, J. L., and Cadet, J. (1995) Reaction of singlet oxygen with 2′-deoxyguanosine and DNA. Isolation and characterization of the main oxidation products. *Chem. Res. Toxicol.* **8,** 379–388
24. Fleming, A. M., Orendt, A. M., He, Y., Zhu, J., Dukor, R. K., and Burrows, C. J. (2013) Reconciliation of chemical, enzymatic, spectroscopic, and computational data to assign the absolute configuration of the DNA base lesion spiroiminodihydantoin. *J. Am. Chem. Soc.* **135,** 18191–18204
25. Khutsishvili, I., Zhang, N., Marky, L. A., Crean, C., Patel, D. J., Geacintov, N. E., and Shafirovich, V. (2013) Thermodynamic profiles and nuclear magnetic resonance studies of oligonucleotide duplexes containing single diastereomeric spiroiminodihydantoin lesions. *Biochemistry* **52,** 1354–1363
26. Jia, L., Shafirovich, V., Shapiro, R., Geacintov, N. E., and Broyde, S. (2006) Flexible 5-guanidino-4-nitroimidazole DNA lesions: structures and thermodynamics. *Biochemistry* **45,** 6644–6655
27. Henderson, P. T., Delaney, J. C., Muller, J. G., Neeley, W. L., Tannenbaum, S. R., Burrows, C. J., and Essigmann, J. M. (2003) The hydantoin lesions formed from oxidation of 7,8-dihydro-8-oxoguanine are potent sources of replication errors *in vivo*. *Biochemistry* **42,** 9257–9262
28. Hailer, M. K., Slade, P. G., Martin, B. D., and Sugden, K. D. (2005) Nei deficient *Escherichia coli* are sensitive to chromate and accumulate the oxidized guanine lesion spiroiminodihydantoin. *Chem. Res. Toxicol.* **18,** 1378–1383
29. Mangerich, A., Knutson, C. G., Parry, N. M., Muthupalani, S., Ye, W., Prestwich, E., Cui, L., McFaline, J. L., Mobley, M., Ge, Z., Taghizadeh, K., Wishnok, J. S., Wogan, G. N., Fox, J. G., Tannenbaum, S. R., and Dedon, P. C. (2012) Infection-induced colitis in mice causes dynamic and tissue-specific changes in stress response and DNA damage leading to colon cancer. *Proc. Natl. Acad. Sci. U.S.A.* **109,** E1820–E1829
30. Leipold, M. D., Muller, J. G., Burrows, C. J., and David, S. S. (2000) Removal of hydantoin products of 8-oxoguanine oxidation by the *Escherichia coli* DNA repair enzyme, FPG. *Biochemistry* **39,** 14984–14992
31. Hazra, T. K., Muller, J. G., Manuel, R. C., Burrows, C. J., Lloyd, R. S., and Mitra, S. (2001) Repair of hydantoins, one electron oxidation product of 8-oxoguanine, by DNA glycosylases of *Escherichia coli*. *Nucleic Acids Res.* **29,** 1967–1974
32. Hailer, M. K., Slade, P. G., Martin, B. D., Rosenquist, T. A., and Sugden, K. D. (2005) Recognition of the oxidized lesions spiroiminodihydantoin and guanidinohydantoin in DNA by the mammalian base excision repair glycosylases NEIL1 and NEIL2. *DNA Repair* **4,** 41–50
33. Liu, M., Bandaru, V., Bond, J. P., Jaruga, P., Zhao, X., Christov, P. P., Burrows, C. J., Rizzo, C. J., Dizdaroglu, M., and Wallace, S. S. (2010) The mouse ortholog of NEIL3 is a functional DNA glycosylase *in vitro* and *in vivo*. *Proc. Natl. Acad. Sci. U.S.A.* **107,** 4925–4930
34. Sejersted, Y., Hildrestrand, G. A., Kunke, D., Rolseth, V., Krokeide, S. Z., Neurauter, C. G., Suganthan, R., Atneosen-Åsegg, M., Fleming, A. M., Saugstad, O. D., Burrows, C. J., Luna, L., and Bjørås, M. (2011) Endonuclease VIII-like 3 (Neil3) DNA glycosylase promotes neurogenesis induced by hypoxia-ischemia. *Proc. Natl. Acad. Sci. U.S.A.* **108,** 18802–18807
35. Liu, M., Imamura, K., Averill, A. M., Wallace, S. S., and Doublié, S. (2013) Structural characterization of a mouse ortholog of human NEIL3 with a marked preference for single-stranded DNA. *Structure* **21,** 247–256
36. Rolseth, V., Krokeide, S. Z., Kunke, D., Neurauter, C. G., Suganthan, R., Sejersted, Y., Hildrestrand, G. A., Bjørås, M., and Luna, L. (2013) Loss of Neil3, the major DNA glycosylase activity for removal of hydantoins in single-stranded DNA, reduces cellular proliferation and sensitizes cells to genotoxic stress. *Biochim. Biophys. Acta* **1833,** 1157–1164
37. Krishnamurthy, N., Zhao, X., Burrows, C. J., and David, S. S. (2008) Superior removal of hydantoin lesions relative to other oxidized bases by the human DNA glycosylase hNEIL1. *Biochemistry* **47,** 7137–7146
38. Zhao, X., Krishnamurthy, N., Burrows, C. J., and David, S. S. (2010) Mutation versus repair: NEIL1 removal of hydantoin lesions in single-stranded, bulge, bubble, and duplex DNA contexts. *Biochemistry* **49,** 1658–1666
39. Krokeide, S. Z., Laerdahl, J. K., Salah, M., Luna, L., Cederkvist, F. H., Fleming, A. M., Burrows, C. J., Dalhus, B., and Bjørås, M. (2013) Human NEIL3 is mainly a monofunctional DNA glycosylase removing spiroimindiohydantoin and guanidinohydantoin. *DNA Repair* **12,** 1159–1164
40. McKibbin, P. L., Fleming, A. M., Towheed, M. A., Van Houten, B., Burrows, C. J., and David, S. S. (2013) Repair of hydantoin lesions and their amine adducts in DNA by base and nucleotide excision repair. *J. Am. Chem. Soc.* **135,** 13851–13861
41. Dimitri, A., Jia, L., Shafirovich, V., Geacintov, N. E., Broyde, S., and Scicchitano, D. A. (2008) Transcription of DNA containing the 5-guanidino-4-nitroimidazole lesion by human RNA polymerase II and bacteriophage T7 RNA polymerase. *DNA Repair* **7,** 1276–1288
42. Mocquet, V., Kropachev, K., Kolbanovskiy, M., Kolbanovskiy, A., Tapias, A., Cai, Y., Broyde, S., Geacintov, N. E., and Egly, J. M. (2007) The human DNA repair factor XPC-HR23B distinguishes stereoisomeric benzo[a]pyrenyl-DNA lesions. *EMBO J.* **26,** 2923–2932
43. Hess, M. T., Gunz, D., Luneva, N., Geacintov, N. E., and Naegeli, H. (1997) Base pair conformation-dependent excision of benzo[a]pyrene diol epoxide-guanine adducts by human nucleotide excision repair enzymes. *Mol. Cell. Biol.* **17,** 7069–7076
44. Mao, B., Xu, J., Li, B., Margulis, L. A., Smirnov, S., Ya, N. Q., Courtney, S. H., and Geacintov, N. E. (1995) Synthesis and characterization of covalent adducts derived from the binding of benzo[a]pyrene diol expoxide to a -GGG- sequence in a deoxyoligonucleotide. *Carcinogenesis* **16,** 357–365
45. Lee, Y. C., Cai, Y., Mu, H., Broyde, S., Amin, S., Chen, X., Min, J. H., and Geacintov, N. E. (2014) The relationships between XPC binding to conformationally diverse DNA adducts and their excision by the human NER system: is there a correlation? *DNA Repair* **19,** 55–63
46. Min, J. H., and Pavletich, N. P. (2007) Recognition of DNA damage by the Rad4 nucleotide excision repair protein. *Nature* **449,** 570–575
47. Rosenquist, T. A., Zaika, E., Fernandes, A. S., Zharkov, D. O., Miller, H., and Grollman, A. P. (2003) The novel DNA glycosylase, NEIL1, protects mammalian cells from radiation-mediated cell death. *DNA Repair* **2,** 581–591
48. Porello, S. L., Leyes, A. E., and David, S. S. (1998) Single-turnover and pre-steady-state kinetics of the reaction of the adenine glycosylase MutY with mismatch-containing DNA substrates. *Biochemistry* **37,** 14756–14764
49. Maiti, A. K., Boldogh, I., Spratt, H., Mitra, S., and Hazra, T. K. (2008) Mutator phenotype of mammalian cells due to deficiency of NEIL1 DNA glycosylase, an oxidized base-specific repair enzyme. *DNA Repair* **7,** 1213–1220
50. Kropachev, K., Kolbanovskii, M., Cai, Y., Rodríguez, F., Kolbanovskii, A., Liu, Y., Zhang, L., Amin, S., Patel, D., Broyde, S., and Geacintov, N. E. (2009) The sequence dependence of human nucleotide excision repair efficiencies of benzo[a]pyrene-derived DNA lesions: insights into the structural factors that favor dual incisions. *J. Mol. Biol.* **386,** 1193–1203
51. Wood, R. D., Robins, P., and Lindahl, T. (1988) Complementation of the xeroderma pigmentosum DNA repair defect in cell-free extracts. *Cell* **53,** 97–106
52. Huang, J. C., Hsu, D. S., Kazantsev, A., and Sancar, A. (1994) Substrate spectrum of human excinuclease: repair of abasic sites, methylated bases, mismatches, and bulky adducts. *Proc. Natl. Acad. Sci. U.S.A.* **91,** 12213–12217
53. Gillet, L. C., and Schärer, O. D. (2006) Molecular mechanisms of mammalian global genome nucleotide excision repair. *Chem. Rev.* **106,** 253–276
54. Wallace, S. S., Murphy, D. L., and Sweasy, J. B. (2012) Base excision repair and cancer. *Cancer Lett.* **327,** 73–89
55. Sugasawa, K., Okamoto, T., Shimizu, Y., Masutani, C., Iwai, S., and Hanaoka, F. (2001) A multistep damage recognition mechanism for global genomic nucleotide excision repair. *Genes Dev.* **15,** 507–521
56. Huang, J. C., Svoboda, D. L., Reardon, J. T., and Sancar, A. (1992) Human nucleotide excision nuclease removes thymine dimers from DNA by incising the 22nd phosphodiester bond 5′ and the 6th phosphodiester bond 3′ to the photodimer. *Proc. Natl. Acad. Sci. U.S.A.* **89,** 3664–3668
57. Huang, J. C., and Sancar, A. (1994) Determination of minimum substrate size for human excinuclease. *J. Biol. Chem.* **269,** 19034–19040
58. Mao, B., Li, B., Amin, S., Cosman, M., and Geacintov, N. E. (1993) Oppo-

site stereoselective resistance to digestion by phosphodiesterases I and II of benzo[a]pyrene diol epoxide-modified oligonucleotide adducts. *Biochemistry* **32,** 11785–11793
59. Leipold, M. D., Workman, H., Muller, J. G., Burrows, C. J., and David, S. S. (2003) Recognition and removal of oxidized guanines in duplex DNA by the base excision repair enzymes hOGG1, yOGG1, and yOGG2. *Biochemistry* **42,** 11373–11381
60. Maher, R. L., Prasad, A., Rizvanova, O., Wallace, S. S., and Pederson, D. S. (2013) Contribution of DNA unwrapping from histone octamers to the repair of oxidatively damaged DNA in nucleosomes. *DNA Repair* **12,** 964–971
61. Muftuoglu, M., de Souza-Pinto, N. C., Dogan, A., Aamann, M., Stevnsner, T., Rybanska, I., Kirkali, G., Dizdaroglu, M., and Bohr, V. A. (2009) Cockayne syndrome group B protein stimulates repair of formamidopyrimidines by NEIL1 DNA glycosylase. *J. Biol. Chem.* **284,** 9270–9279
62. Aamann, M. D., Hvitby, C., Popuri, V., Muftuoglu, M., Lemminger, L., Skeby, C. K., Keijzers, G., Ahn, B., Bjørås, M., Bohr, V. A., and Stevnsner, T. (2014) Cockayne syndrome group B protein stimulates NEIL2 DNA glycosylase activity. *Mech. Ageing Dev.* **135,** 1–14
63. Liu, M., Doublié, S., and Wallace, S. S. (2013) Neil3, the final frontier for the DNA glycosylases that recognize oxidative damage. *Mutat. Res.* **743,** 4–11
64. Hazra, T. K., Izumi, T., Boldogh, I., Imhoff, B., Kow, Y. W., Jaruga, P., Dizdaroglu, M., and Mitra, S. (2002) Identification and characterization of a human DNA glycosylase for repair of modified bases in oxidatively damaged DNA. *Proc. Natl. Acad. Sci. U.S.A.* **99,** 3523–3528
65. Bandaru, V., Sunkara, S., Wallace, S. S., and Bond, J. P. (2002) A novel human DNA glycosylase that removes oxidative DNA damage and is homologous to *Escherichia coli* endonuclease VIII. *DNA Repair* **1,** 517–529
66. Hazra, T. K., Kow, Y. W., Hatahet, Z., Imhoff, B., Boldogh, I., Mokkapati, S. K., Mitra, S., and Izumi, T. (2002) Identification and characterization of a novel human DNA glycosylase for repair of cytosine-derived lesions. *J. Biol. Chem.* **277,** 30417–30420
67. Morland, I., Rolseth, V., Luna, L., Rognes, T., Bjørås, M., and Seeberg, E. (2002) Human DNA glycosylases of the bacterial Fpg/MutM superfamily: an alternative pathway for the repair of 8-oxoguanine and other oxidation products in DNA. *Nucleic Acids Res.* **30,** 4926–4936
68. Dobson, C. J., and Allinson, S. L. (2006) The phosphatase activity of mammalian polynucleotide kinase takes precedence over its kinase activity in repair of single strand breaks. *Nucleic Acids Res.* **34,** 2230–2237
69. Wiederhold, L., Leppard, J. B., Kedar, P., Karimi-Busheri, F., Rasouli-Nia, A., Weinfeld, M., Tomkinson, A. E., Izumi, T., Prasad, R., Wilson, S. H., Mitra, S., and Hazra, T. K. (2004) AP endonuclease-independent DNA base excision repair in human cells. *Mol. Cell* **15,** 209–220
70. Talhaoui, I., Shafirovich, V., Liu, Z., Saint-Pierre, C., Akishev, Z., Matkarimov, B. T., Gasparutto, D., Geacintov, N. E., and Saparbaev, M. (2015) Oxidatively generated guanine(C8)-thymine(N3) intrastrand cross-links in double-stranded DNA are repaired by base excision repair pathways. *J. Biol. Chem.* **290,** 14610–14617
71. Luijsterburg, M. S., von Bornstaedt, G., Gourdin, A. M., Politi, A. Z., Moné, M. J., Warmerdam, D. O., Goedhart, J., Vermeulen, W., van Driel, R., and Höfer, T. (2010) Stochastic and reversible assembly of a multiprotein DNA repair complex ensures accurate target site recognition and efficient repair. *J. Cell Biol.* **189,** 445–463
72. Riedl, T., Hanaoka, F., and Egly, J. M. (2003) The comings and goings of nucleotide excision repair factors on damaged DNA. *EMBO J.* **22,** 5293–5303
73. Sugasawa, K., Ng, J. M., Masutani, C., Iwai, S., van der Spek, P. J., Eker, A. P., Hanaoka, F., Bootsma, D., and Hoeijmakers, J. H. (1998) Xeroderma pigmentosum group C protein complex is the initiator of global genome nucleotide excision repair. *Mol. Cell* **2,** 223–232
74. Naegeli, H., and Sugasawa, K. (2011) The xeroderma pigmentosum pathway: decision tree analysis of DNA quality. *DNA Repair* **10,** 673–683
75. Schärer, O. D. (2013) Nucleotide excision repair in eukaryotes. *Cold Spring Harb. Perspect. Biol.* **5,** a012609
76. Marteijn, J. A., Lans, H., Vermeulen, W., and Hoeijmakers, J. H. (2014) Understanding nucleotide excision repair and its roles in cancer and ageing. *Nat. Rev. Mol. Cell Biol.* **15,** 465–481
77. Miura, N., Miyamoto, I., Asahina, H., Satokata, I., Tanaka, K., and Okada, Y. (1991) Identification and characterization of xpac protein, the gene product of the human XPAC (xeroderma pigmentosum group A complementing) gene. *J. Biol. Chem.* **266,** 19786–19789
78. Kuraoka, I., Bender, C., Romieu, A., Cadet, J., Wood, R. D., and Lindahl, T. (2000) Removal of oxygen free-radical-induced 5′,8-purine cyclodeoxynucleosides from DNA by the nucleotide excision-repair pathway in human cells. *Proc. Natl. Acad. Sci. U.S.A.* **97,** 3832–3837
79. Saijo, M., Matsuda, T., Kuraoka, I., and Tanaka, K. (2004) Inhibition of nucleotide excision repair by anti-XPA monoclonal antibodies which interfere with binding to RPA, ERCC1, and TFIIH. *Biochem. Biophys. Res. Commun.* **321,** 815–822
80. Shen, J. C., Fox, E. J., Ahn, E. H., and Loeb, L. A. (2014) A rapid assay for measuring nucleotide excision repair by oligonucleotide retrieval. *Sci. Rep.* **4,** 4894
81. Luo, W., Muller, J. G., Rachlin, E. M., and Burrows, C. J. (2001) Characterization of hydantoin products from one-electron oxidation of 8- oxo-7,8-dihydroguanosine in a nucleoside model. *Chem. Res. Toxicol.* **14,** 927–938
82. Aller, P., Ye, Y., Wallace, S. S., Burrows, C. J., and Doublié, S. (2010) Crystal structure of a replicative DNA polymerase bound to the oxidized guanine lesion guanidinohydantoin. *Biochemistry* **49,** 2502–2509
83. Eckenroth, B. E., Fleming, A. M., Sweasy, J. B., Burrows, C. J., and Doublié, S. (2014) Crystal structure of DNA polymerase β with DNA containing the base lesion spiroiminodihydantoin in a templating position. *Biochemistry* **53,** 2075–2077
84. Jia, L., Shafirovich, V., Shapiro, R., Geacintov, N. E., and Broyde, S. (2005) Structural and thermodynamic features of spiroiminodihydantoin damaged DNA duplexes. *Biochemistry* **44,** 13342–13353
85. Yennie, C. J., and Delaney, S. (2012) Thermodynamic consequences of the hyperoxidized guanine lesion guanidinohydantoin in duplex DNA. *Chem. Res. Toxicol.* **25,** 1732–1739
86. Jin, Q., Fleming, A. M., Ding, Y., Burrows, C. J., and White, H. S. (2013) Structural destabilization of DNA duplexes containing single-base lesions investigated by nanopore measurements. *Biochemistry* **52,** 7870–7877
87. Neeley, W. L., Henderson, P. T., and Essigmann, J. M. (2004) Efficient synthesis of DNA containing the guanine oxidation-nitration product 5-guanidino-4-nitroimidazole: generation by a postsynthetic substitution reaction. *Org. Lett.* **6,** 245–248
88. Duarte, V., Muller, J. G., and Burrows, C. J. (1999) Insertion of dGMP and dAMP during *in vitro* DNA synthesis opposite an oxidized form of 7,8-dihydro-8-oxoguanine. *Nucleic Acids Res.* **27,** 496–502